Coordinated Dispatch Based on Distributed Robust Optimization for Interconnected Urban Integrated Energy and Transmission Systems

Wei Xu, Yufeng Guo, Tianhui Meng, Yingwei Wang, and Jilai Yu

***Abstract*—To improve the economic efficiency of urban integrated energy systems (UIESs) and mitigate day-ahead dispatch uncertainty, this paper presents an interconnected UIES and transmission system (TS) model based on distributed robust optimization. First, interconnections are established between a TS and multiple UIESs, as well as among different UIESs, each incorporating multiple energy forms. The Bregman alternating direction method with multipliers (BADMM) is then applied to multi-block problems, ensuring the privacy of each energy system operator (ESO). Second, robust optimization based on wind probability distribution information is implemented for each ESO to address dispatch uncertainty. The column and constraint generation (C&CG) algorithm is then employed to solve the robust model. Third, to tackle the convergence and practicability issues overlooked in the existing studies, an external C&CG with an internal BADMM and corresponding acceleration strategy is devised. Finally, numerical results demonstrate that the adoption of the proposed model and method for absorbing wind power and managing its uncertainty results in economic benefits.**

***Index Terms*—Distributed robust optimization, distributionally robust dispatch, urban integrated energy system, transmission system, external column and constraint generation (C&CG), internal Bregman alternating direction method with multipliers (BADMM).**

NOMENCLATURE

A. Indices and Sets

Ψ^{ts}, Ψ^{us}	Sets of transmission systems (TSs) and urban integrated energy systems (UIESs)
Ω^{ts}, Ω_k^{us}	Sets of probabilities of wind scenarios in TS and $UIES_k$
Ω_{HB}, Ω_{NHB}	Sets of heat sources and load nodes in UIES
Ω_S, Ω_R	Sets of heat supplies and return pipelines in UIES
Ω_{Se}, Ω_{Ss}	Sets of heat supply pipelines with node o as end and starting points
Ω_G	Set of all nodes in gas network
Ω_{GC}, Ω_{NGC}	Sets of gas branches with and without compressors
Ω_{Re}, Ω_{Rs}	Sets of heat return pipelines with node o as end and starting points
bu	Index of gas purchase nodes of UIES
B_k, M_k	Sets of gas purchase and gas load nodes in $UIES_k$
d, hd, gd	Indices of electrical, heat, and gas loads in UIES
e, b, g	Indices of electrical boiler (EB), gas boiler (GB), and gas turbine (GT)
$G(m)$	Set of components connected to gas node m
hs	Index of heat sources
ij, mn, hf	Indices of distribution lines, gas pipelines, and heat pipelines in UIES
j, h	Indices of electrical and heat nodes in UIES
m, n, l	Indices of gas nodes
k, u	Indices of UIESs, denoting as $UIES_k$ and $UIES_u$
R^{ts}, R^{us}	Sets of wind scenarios in TS and UIES
s, z	Indices of iterations for Bregman alternating direction method with multipliers (BADMM) and column and constraint generation (C&CG)
t	Index of time periods
tm	Index of generators in TS
w, v	Indices of energy production and conversion equipment

B. Parameters

α_1, α_∞	Uncertainty probability confidence values for 1-norm and ∞-norm constraints
$\alpha_{m,t}^{buy}$	Intraday gas purchase volume variation limit from day-ahead plan
$\alpha_{w,t}^{tra}$	Intraday output variation limit from day-ahead plan for energy conversion devices

Manuscript received: May 4, 2023; revised: July 31, 2023; accepted: September 20, 2023. Date of CrossCheck: September 20, 2023. Date of online publication: March 5, 2024.

This work was supported by the Science and Technology Project of State Grid Corporation of China (No. 5108-202299259A-1-0-ZB).

W. Xu, Y. Guo (corresponding author), T. Meng, Y. Wang, and J. Yu are with the School of Electrical Engineering and Automation, Harbin Institute of Technology, Harbin 150001, China (e-mail: xuweing@foxmail.com; guoyufeng@hit.edu.cn; mtianhui.hit@foxmail.com; 13322482011@163.com; yupwrs@hit.edu.cn).

DOI: 10.35833/MPCE.2023.000255

ε_{ccg}	Convergence tolerance of C&CG algorithm
$\varepsilon_{\mathrm{P}}^{(s)}$, $\varepsilon_{\mathrm{D}}^{(s)}$	Primal and dual residuals in the s^{th} iteration of BADMM algorithm
θ_1, θ_∞	Allowable probability deviation limits under 1-norm and ∞-norm constraints
κ	Compressor factor
ρ	Penalty parameter of Lagrange function
ρ_{w}, c	Water density and specific heat capacity
τ_{pipe}	Water transmission time of *hf*
$\Delta P_{m,t}^{\mathrm{cr,max}}$	Limit value of gas pressure change during adjacent periods
$\Delta P_{m,t}^{\mathrm{dr,max}}$	Limit value of gas pressure change in intraday stage relative to day-ahead stage
$\Delta T_{h,t}^{\mathrm{sl,max}}$	Limit value of temperature change during adjacent periods
$\Delta T_{h,t}^{\mathrm{ch,max}}$	Limit value of temperature change in intraday stage relative to day-ahead stage
$\Delta Q_{m,t}^{\mathrm{gl,max}}$, $\Delta Q_{m,t}^{\mathrm{gl,min}}$	Upper and lower bounds of gas load curtailment
C_{mn}	Weymouth coefficient of *mn*
gap_{P}, gap_{D}	Convergence tolerance of primal and dual residuals of BADMM
$H_{hd,t}^{\mathrm{hl,p}}$, $Q_{m,t}^{\mathrm{gl,p}}$	Predictive heat and gas loads
L_{hf}, d_{hf}	Length and diameter of *hf*
M, R	Numbers of selected wind samples and extracted scenarios
$m_{hd,t}$, $m_{hs,t}$, $m_{hf,t}$	Water mass flow rates of heat load, heat source, and heat pipeline
$p_n^{\max}$, $p_n^{\min}$	Upper and lower pressure limits of gas node *n*
$P_{k,\max}^{\mathrm{tu}}$, $P_{ku,\max}^{\mathrm{uu}}$	The maximum capacities of tie lines between TS and UIES$_k$, and UIES$_k$ and UIES$_u$
$Q_{\min}^{\mathrm{buy}}$, $Q_{\max}^{\mathrm{buy}}$	The minimum and maximum gas purchase volumes
$U_{tm,t}^{\mathrm{th}}$, $D_{tm,t}^{\mathrm{th}}$	Ramp up and down rate limits of generator

C. Superscripts

0	Variable and parameter of day-ahead stage
*	Optimal result of variables or functions
pro	Unified representation of energy production equipment such as GT and GB
r	Variable and parameter of the r^{th} intraday wind scenario
tra	Unified representation of energy conversion equipment such as waste heat boiler (WHB) and EB
ts, us	Variables and parameters of TS and UIES
+, –	Increment and decreament of volume

D. Variables

η^{ts}, η_k^{us}	Auxiliary variables replacing objectives of TS and UIES$_k$ subproblems
$\Delta P_{v,t}^{\mathrm{pro}}$, $\Delta P_{w,t}^{\mathrm{tra}}$	Intraday output variation of energy production equipment and energy conversion equipment
$\Delta P_{v,t}^{\mathrm{pro,+}}$, $\Delta P_{v,t}^{\mathrm{pro,-}}$	Output increment and decrement of energy production equipment
$\Delta P_{w,t}^{\mathrm{tra,+}}$, $\Delta P_{w,t}^{\mathrm{tra,-}}$	Output increment and decrement of energy conversion equipment
$\Delta H_{hd,t}^{\mathrm{hl}}$, $\Delta Q_{m,t}^{\mathrm{gl}}$	Heat and gas load curtailments in UIES
$\Delta P_{d,t}^{\mathrm{el}}$, $\Delta P_{j,t}^{\mathrm{el}}$	Electrical load curtailments in TS and UIES
$\Delta P_{tm,t}^{\mathrm{th}}$	Generator output volume variation
$\Delta Q_{m,t}^{\mathrm{buy}}$	Gas purchase volume variation
$H_{hd,t}^{\mathrm{hl}}$, $Q_{m,t}^{\mathrm{gl}}$	Dispatched heat and gas loads
$H_{hs,t}^{\mathrm{ss}}$	Heat power of heat source
$P_{k,t}^{\mathrm{tu}}$, $P_{k,t}^{\mathrm{ut}}$	Power on both sides of tie line between TS and UIES$_k$
$P_{ku,k,t}^{\mathrm{uu}}$, $P_{ku,u,t}^{\mathrm{uu}}$	Power on both sides of tie line between UIES$_k$ and UIES$_u$
$P_{g,t}^{\mathrm{gt}}$, $P_{tm,t}^{\mathrm{th}}$	Power outputs of GT and generator
$p_{n,t}$, $p_{m,t}$	Gas nodal pressures
p_r	Probability of the r^{th} intraday wind scenario
$Q_{mn,t}$	Gas flow of *mn*
$Q_{bu,t}^{\mathrm{buy}}$	Gas purchase volume plan
$Q_{g,t}^{\mathrm{gt}}$, $Q_{b,t}^{\mathrm{gb}}$	Gas inputs of GT and GB
$Q_{gd,t}^{\mathrm{gl}}$	Dispatched gas load
$R_{tm,t}^{\mathrm{gu}}$, $R_{tm,t}^{\mathrm{gd}}$	Dispatched up and down reserves of generator in TS
$R_{v,t}^{\mathrm{prou}}$, $R_{v,t}^{\mathrm{prod}}$	Dispatched up and down reserves of production equipment in UIES
$T_{hf,t}^{\mathrm{outs}}$, $T_{hf,t}^{\mathrm{ins}}$	Temperatures at outlet and inlet of supply pipelines
$T_{hf,t}^{\mathrm{outr}}$, $T_{hf,t}^{\mathrm{inr}}$	Temperatures at outlet and inlet of return pipelines
$T_{hf,t}^{\mathrm{out},0}$, $T_{hf,t}^{\mathrm{in},0}$	Outlet and inlet temperatures of *hf*
$T_{hs,t}^{\mathrm{ss}}$, $T_{hs,t}^{\mathrm{sr}}$	Temperatures of heat source nodes in heat supply and return pipelines
$T_{hd,t}^{\mathrm{ls}}$, $T_{hd,t}^{\mathrm{lr}}$	Temperatures of heat load nodes in heat supply and return pipelines
$T_{o,t}^{\mathrm{mixs}}$, $T_{o,t}^{\mathrm{mixr}}$	Mixed temperatures at node *o* in heat supply and return pipelines

E. Vectors

$\boldsymbol{\gamma}$	Lagrange multiplier
$\boldsymbol{\mu}^{\mathrm{ts}}$, $\boldsymbol{\mu}_k^{\mathrm{us}}$	Wind scenario parameters for TS and UIES$_k$
$\boldsymbol{A}$, $\boldsymbol{B}$	Coefficient matrices for coupling constraints
$\boldsymbol{G}$, $\boldsymbol{g}$	Functions corresponding to all constraints of master problem (MP) for TS and upper bounds
$\boldsymbol{H}$, $\boldsymbol{h}$	Functions corresponding to all constraints of MP for UIES$_k$ and upper bounds
$\boldsymbol{p}^{\mathrm{ts}}$, $\boldsymbol{p}_k^{\mathrm{us}}$	Probability distribution variables for wind scenarios in TS and UIES$_k$
$\boldsymbol{x}^{\mathrm{ts}}$, $\boldsymbol{x}_k^{\mathrm{us}}$	Day-ahead problem variables for TS and UIES$_k$
$\boldsymbol{y}^{\mathrm{ts}}$, $\boldsymbol{y}_k^{\mathrm{us}}$	Intraday problem variables for TS and UIES$_k$

I. Introduction

As distributed generation (DG) sources have become prevalent in urban integrated energy systems (UIESs), both active energy suppliers and distributors operate in urban areas to serve consumers. The optimal utilization of regulating resources can be achieved through holistic interconnection strategies between UIESs and transmission systems (TSs), facilitating new energy surplus absorption and mitigating weak system stability. Moreover, the coupling of diverse energy sources such as electricity, gas, and heat is becoming increasingly complex, with various energy conversions enabling the full utilization of new energy resources.

Current research works on energy system coordination are primarily divided into two categories: collaboration between integrated energy systems (IESs) and collaboration within TSs and distribution systems. References [1] and [2] propose a distributed dispatch strategy for joint transmission and distribution optimization considering distribution system flexibility. Reference [3] presents a cooperative optimal dispatch of TSs and distribution systems based on a two-stage robust optimization (RO), leveraging the adjustment capacity of TSs and distribution systems for wind power intermittency and uncertainty. References [4] and [5] utilize the alternating target cascade (ATC) algorithm for coordination among microgrids, accounting for renewable energy uncertainty. Reference [6] shows that the interconnected dispatch of energy systems across regions using distributed algorithms, and RO enhances the economy of the entire system. In previous studies which examine the interconnection of TSs and distribution system, the emphasis is largely on the coupling of power energy, overlooking the growing integration of multiple energy sources in urban distribution systems. Consequently, by concurrently considering the connections between TS and multiple UIESs and the interconnections among different UIESs [7], we can ensure the thorough utilization of diverse energy resources and foster mutual support among energy systems.

The coordinated optimization of different subsystems often encounters privacy protection challenges, prompting the use of distributed methods for interregional coordination. These methods typically require minimal interregional interaction variables. Notable examples include ATC algorithm [8], [9] and the alternating direction multiplier method (ADMM) [10]-[12]. However, these algorithms and methods primarily involve information-flow interactions between two parties or levels, essentially addressing "2-block" problems or their combinations. The convergence for "*N*-block" problems can be challenging [13]. Reference [14] extends the ADMM and proposes the prediction-correction-based ADMM (PCB-ADMM) to solve multiple separable problems. This method has been applied to collaborative optimization of electrical-gas-heat system [15] and coordination of transmission system operator and distribution system operator (TSO-DSO) [16]. Nevertheless, the acceleration of multi-block distributed algorithms remains a promising avenue for further research. A comparison between proposed and state-of-the-art methods is presented in Table I, where ARO is short for adaptive RO.

TABLE I
Comparisons Between Proposed and State-of-the-art Methods

Reference	System modeling				Uncertainty modeling	Method		Accelerated strategy	Multi-block
	Transmission	Distribution	Gas	Heat		Outer	Inner		
[3]	√	√	×	×	RO	ADMM	C&CG	√	×
[4]	×	√	×	×	RO	ATC	C&CG	×	×
[6]	×	√	√	√	RO	ADMM	C&CG	×	×
[7]	×	√	√	√	RO	ADMM	C&CG	×	×
[8]	×	√	√	√	RO	ATC	C&CG	×	×
[11]	√	×	√	×	RO	ADMM	-	×	×
[12]	√	√	×	×	SO	ADMM	-	×	×
[15]	×	√	√	√	RO	PCB-ADMM	C&CG	×	√
[17]	×	√	×	×	ARO	AUP	ADMM	×	×
This paper	√	√	√	√	DRO	C&CG	BADMM	√	√

Note: √ and × indicate whether the item is considered in the listed references, respectively.

The day-ahead dispatch optimization of energy systems has garnered considerable research attention. As a myriad of new energy sources connected to the power grid, distributionally robust optimization (DRO) has emerged as a research area that addresses the uncertainty arising from these new energy sources. DRO synergizes the advantages of stochastic and RO methods, reflecting the probability distribution information of new energy sources while maintaining conservativeness. In [18], a fuzzy set of wind power prediction errors is constructed based on historical wind power moment information, and a coupled DRO dispatch model of an electricity-gas system is established using dual transformation. Reference [19] investigates generalized energy storage resources within a park-level IES and develops a DRO model based on the Wasserstein distance [20] to address wind power uncertainty. Reference [21] employs a data-driven distributed robust method to optimize the reactive power in a distribution system. UIESs involve numerous energy networks, resulting in mathematical models with numerous constraint variables. Conventional RO [22], [23] requires dual transformation of the inner-layer problem by introducing numerous non-convex terms. DRO based on the Wasserstein distance

requires that multiple scenarios should be considered. Due to computational resource constraints, few studies have been conducted on robust IES dispatch while considering network dynamics. The data-driven method requires only the probability information of typical scenarios and avoids complex dual transformations, making it suitable for intricate models.

The column-and-constraint generation (C&CG) algorithm [24] is commonly used to solve the two-stage RO. Several studies have combined distributed algorithms with the C&CG algorithm. Reference [25] integrates the ATC and C&CG algorithms for hierarchical and robust dispatch in AC/DC hybrid systems. Reference [26] combines the ADMM and C&CG algorithms to address the voltage optimization problem. In these studies, the distributed algorithm serves as the external framework, and the C&CG algorithm is the specific solution framework for each iteration [27], [28]. However, the solution process does not ensure convergence. The main reason for this is that the worst-case-scenario set of the master problem (MP) changes after each iteration of C&CG algorithm, meaning that the constraints of each problem solved by the distributed algorithm constantly shift. This makes it difficult to prove that the convergence condition of the distributed algorithm is ultimately achieved. Reference [17] introduces the alternating uncertainty-update procedure (AUP) to overcome the issues mentioned above. Few studies have demonstrated the convergence of distributed algorithms when combined with C&CG.

Based on the aforementioned discussion, the distributed robust joint dispatch of TS and distribution system (DS) faces the following challenges. The urban DS is evolving into a system with deep coupling of multiple energy sources, introducing new dispatch complexities, and the convergence and practicality of the combined distributed and C&CG algorithms still have room for improvement. To address these issues, this paper investigates both the modeling and solution methodologies. The main contributions of this paper are summarized as follows:

1) We introduce a novel interconnected energy system model that expands transmission and distribution dispatch to include multiple energy forms. In this model, the UIES is directly linked to both the TS and other UIESs to further enhance privacy protection and strengthen mutual support capabilities.

2) The Bregman alternating direction method with multipliers (BADMM) is employed to coordinate the dispatches of energy system operators (ESOs) to ensure the privacy of each ESO. The BADMM overcomes the constraints inherent in the traditional ADMM when addressing multi-block problems. The C&CG algorithm is also applied to address the DRO problem of each ESO.

3) To ensure the convergence and practicality of distributed robust dispatch, we devise a framework that nests the internal BADMM in an external C&CG and introduces acceleration strategies based on structural characteristics of the framework. The framework ensures the theoretical convergence of the problem, whereas the strategies enhance the convergence speed.

II. Concept and Structure of Proposed Model

A. Structure of Joint TS and UIESs

Compared with traditional joint transmission and distribution dispatch, two aspects are expanded.

1) Energy diversity expansion: we diversify the urban energy categories by transitioning from sole electrical energy to electrical, gas, and heat energies.

2) UIES interconnection enhancement: UIES establishes connections with TS and other UIESs. The design is used to preserve the confidentiality of each ESO, ensuring that the transactional information between systems is not disclosed to other systems.

In each energy system, there is an ESO for energy planning and trading with other systems. Figure 1 shows the schematic of energy interconnection structure. WT, PV, GT, GB, WHB, and EB are short for wind turbine, photovoltaic, gas turbine, gas boiler, waste heat boiler, and electrical boiler, respectively. Energy is transmitted between systems through tie lines, a data-driven DRO is utilized within each ESO for day-ahead dispatch, and the relevant boundary coupling variable information is transmitted to the coordination dispatch center (CDC) for coordinated dispatch. The CDC is responsible for determining convergence and updating relevant information for all ESOs.

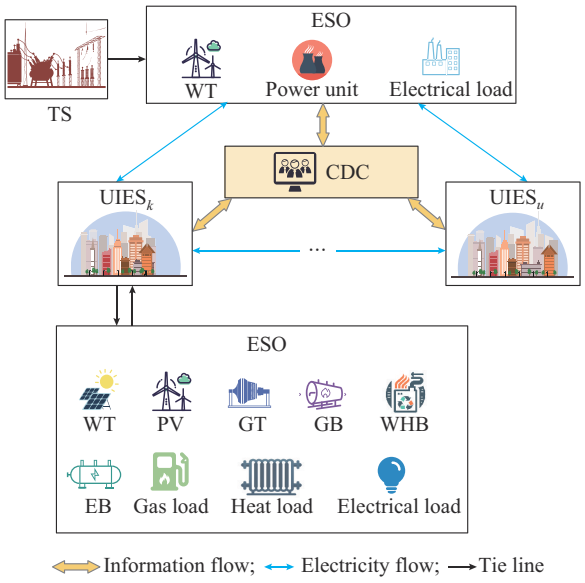

Fig. 1. Schematic of energy interconnection structure.

Coupling constraints between UIES$_k$ and its superior TS and UIES$_u$ can be formulated as:

$$P_{k,t}^{\mathrm{tu},0} = P_{k,t}^{\mathrm{ut},0} \quad \forall k,u \in \Psi^{\mathrm{us}} \tag{1a}$$

$$P_{ku,k,t}^{\mathrm{uu},0} = P_{ku,u,t}^{\mathrm{uu},0} \quad \forall k,u \in \Psi^{\mathrm{us}} \tag{1b}$$

In (1a), the transmited power from the TS to UIES$_k$ is positive, indicating that the TS serves as a virtual power supply and UIES$_k$ as a virtual load. When it is negative, the situation is reversed. The constraint in (1b) is similar to that in (1a), where the subscript *ku* denotes the power transmission from UIES$_k$ to UIES$_u$.

B. Framework of Fuzzy Set and Robust Model

1) Fuzzy Set

In conventional RO, the box uncertainty set characterizes the uncertain variables, leading to overly conservative results.

This paper employs a data-driven DRO algorithm to address conservatism as shown in (2), and p_r satisfies the conditions given in (3).

$$\begin{cases} \Omega_r=\{p_r\} \quad p_r\geq 0, r=1,2,\ldots,R \\ \Omega_r=\{p_r\} \quad \sum_{r=1}^{R} p_r=1 \\ \Omega_r=\{p_r\} \quad \sum_{r=1}^{R}|p_r-p_r^0|\leq\theta_1 \\ \Omega_r=\{p_r\} \quad \max_{1\leq r\leq R}|p_r-p_r^0|\leq\theta_\infty \end{cases} \tag{2}$$

$$\begin{cases} \Pr\left\{\sum_{r\in R}|p_r-p_r^0|\leq\theta_1\right\}\geq 1-2R\mathrm{e}^{-2M\theta_1/R} \\ \Pr\{|p_r-p_r^0|\leq\theta_\infty\}\geq 1-2R\mathrm{e}^{-2M\theta_\infty} \end{cases} \tag{3}$$

Then, θ_1 and θ_∞ satisfy:

$$\begin{cases} \theta_1=\dfrac{R}{2M}\ln\dfrac{2R}{1-\alpha_1} \\ \theta_\infty=\dfrac{1}{2M}\ln\dfrac{2R}{1-\alpha_\infty} \end{cases} \tag{4}$$

2) Robust Model of Entire System

The objective function of the optimal overall cost of the TS and UIESs can be expressed as (5). f^{ts1}, f^{us1} and f^{ts2}, f^{us2} are the objective functions for the day-ahead and intraday stages, respectively.

$$\min_{\boldsymbol{x}^{\mathrm{ts}}}\{f^{\mathrm{ts1}}(\boldsymbol{x}^{\mathrm{ts}})+\max_{\boldsymbol{p}^{\mathrm{ts}}\in\Omega^{\mathrm{ts}}}\min_{\boldsymbol{y}^{\mathrm{ts}}} f^{\mathrm{ts2}}(\boldsymbol{y}^{\mathrm{ts}},\boldsymbol{\mu}^{\mathrm{ts}},\boldsymbol{p}^{\mathrm{ts}})\}+ \min_{\boldsymbol{x}_k^{\mathrm{us}}}\left\{\sum_k(f_k^{\mathrm{us1}}(\boldsymbol{x}_k^{\mathrm{us}})+\max_{\boldsymbol{p}_k^{\mathrm{us}}\in\Omega_k^{\mathrm{us}}}\min_{\boldsymbol{y}_k^{\mathrm{us}}} f_k^{\mathrm{us2}}(\boldsymbol{y}_k^{\mathrm{us}},\boldsymbol{\mu}_k^{\mathrm{us}},\boldsymbol{p}_k^{\mathrm{us}}))\right\} \tag{5}$$

In the two-layer robust dispatch model, the inner layer "max-min", which is based on the day-ahead dispatch plan from the outer layer "min", is optimized to obtain the most beneficial adjustment results in the wind scenarios of adverse probability distribution within the day. The outer layer, based on the adverse intraday wind scenario probability distribution derived from the inner layer, establishes the most cost-efficient day-ahead dispatch plan.

III. TS Model

A. Objective Function

$$\min\left\{\sum_{t\in T}(f_t^{\mathrm{th},0}+f_t^{\mathrm{wp},0}+f_t^{\mathrm{el},0}+f_t^{\mathrm{tr},0})\max_{p_r\in\Omega^{\mathrm{ts}}}\min\sum_{r\in R^{\mathrm{ts}}}p_r\sum_{t\in T}(\Delta f_t^{\mathrm{th},r}+ f_t^{\mathrm{wp},r}+f_t^{\mathrm{el},r})\right\} \tag{6}$$

The specific expression of the objective function is provided in [29]. The day-ahead objective function considers the minimum generator cost $f_t^{\mathrm{th},0}$, wind curtailment $f_t^{\mathrm{wp},0}$, load limit cost $f_t^{\mathrm{el},0}$, and electricity transmission cost $f_t^{\mathrm{tr},0}$. The intraday objective function is the regulation cost, which consists of the generator output adjustment cost $\Delta f_t^{\mathrm{th},r}$, wind curtailment cost $f_t^{\mathrm{wp},r}$, and load curtailment cost $f_t^{\mathrm{el},r}$.

B. Constraints

1) Day-ahead Constraints

The day-ahead constraints of the TS include power balance, generator plan, wind farm plan, load plan, DC current security, and tie-line constraints of TS and UIES. The precise expressions can be found in [29].

2) Intraday Adjustment Constraints

In addition to the constraints obtained by replacing the day-ahead constraint variables with intraday scenario variables, the intraday constraints also consist of fuzzy set constraints (2) - (4) of wind power distribution and adjustment constraints (7) and (8).

$$\begin{cases} P_{tm,t}^{\mathrm{th},r}=P_{tm,t}^{\mathrm{th},0}+\Delta P_{tm,t}^{\mathrm{th},r+}-\Delta P_{tm,t}^{\mathrm{th},r-} \\ P_{tm,t}^{\mathrm{th},0}-R_{tm,t}^{\mathrm{gd}}\leq P_{tm,t}^{\mathrm{th},r}\leq P_{tm,t}^{\mathrm{th},0}+R_{tm,t}^{\mathrm{gu}} \\ -D_{tm,t}^{\mathrm{th}}\Delta t\leq P_{tm,t}^{\mathrm{th},r}-P_{tm,t-1}^{\mathrm{th},r}\leq U_{tm,t}^{\mathrm{th}}\Delta t \end{cases} \tag{7}$$

$$0\leq\Delta P_{d,t}^{\mathrm{el},r}\leq\Delta P_{d,t}^{\mathrm{el},0} \tag{8}$$

IV. UIES Model

We next establish a UIES_k model using one UIES as an example. "k" is the index of UIES. For simplicity, we omit it in the variable representation.

A. Objective Function

$$\min\left\{\sum_{t\in T}(f_t^{\mathrm{buy},0}+f_t^{\mathrm{wp},0}+f_t^{\mathrm{ld},0}+f_t^{\mathrm{tr},0})+\max_{p_r\in\Omega^{\mathrm{us}}}\sum_{r\in R^{\mathrm{us}}}p_r\min(\Delta f_t^{\mathrm{gt},r}+ \Delta f_t^{\mathrm{gb},r}+\Delta f_t^{\mathrm{eb},r}+f_t^{\mathrm{wp},r}+f_t^{\mathrm{ld},r}+\Delta f_t^{\mathrm{buy},r})\right\} \tag{9}$$

The specific expression of the objective function is presented in [29]. The day-ahead objective function considers gas costs $f_t^{\mathrm{buy},0}$, $f_t^{\mathrm{wp},0}$, flexible load dispatch costs $f_t^{\mathrm{ld},0}$, and $f_t^{\mathrm{tr},0}$. The intraday phase responds to wind scenarios of adverse probability distribution by adjusting rapidly adjustable equipment and altering gas purchase volume. The objective function includes production equipment adjustment costs $\Delta f_t^{\mathrm{gt},r}$, $\Delta f_t^{\mathrm{gb},r}$, $\Delta f_t^{\mathrm{eb},r}$, gas purchase adjustment cost $\Delta f_t^{\mathrm{buy},r}$, $f_t^{\mathrm{wp},r}$, and flexible load invocation cost $f_t^{\mathrm{ld},r}$.

B. Day-ahead Constraints

1) DS Constraints

These constraints consist DS and load-related constraints. The precise expressions and undefined variables can be found in [29].

2) Gas Network Constraints

A steady-state equation is employed for the gas network. The UIES_k gas network constraints consist of flow balance constraint (10), nodal pressure constraint (11), gas load limit constraint (12), compressor constraint (13), gas purchase volume constraint (14), and second-order cone programming-relaxed Weymouth equation (15), while this relaxation is not invariably tight but is chosen for its computational efficiency and manageability [30].

$$\sum_{bu\in G(m)} Q_{bu,t}^{\text{buy},0} - \left(\sum_{gd\in G(m)} Q_{gd,t}^{\text{gl},0} + \sum_{g\in G(m)} Q_{g,t}^{\text{gt},0} + \sum_{b\in G(m)} Q_{b,t}^{\text{gb},0} \right) = \sum_n Q_{mn,t}^0 - \sum_l Q_{lm,t}^0 \quad \forall m \in \Omega_{\text{G}} \tag{10}$$

$$p_m^{\min} \le p_{m,t}^0 \le p_m^{\max} \quad \forall m \in \Omega_{\text{G}} \tag{11}$$

$$\begin{cases} \Delta Q_{m,t}^{\text{gl},\min} \le \Delta Q_{m,t}^{\text{gl},0} \le \Delta Q_{m,t}^{\text{gl},\max} \\ Q_{m,t}^{\text{gl},0} = Q_{m,t}^{\text{gl,p}} - \Delta Q_{m,t}^{\text{gl},0} \end{cases} \quad \forall m \in M_k \tag{12}$$

$$p_{m,t}^0 \le p_{n,t}^0 \le \kappa p_{m,t}^0 \quad \forall mn \in \Omega_{\text{GC}} \tag{13}$$

$$Q_{\min}^{\text{buy}} \le Q_{bu,t}^{\text{buy},0} \le Q_{\max}^{\text{buy}} \quad \forall bu \in B_k \tag{14}$$

$$\begin{cases} \| Q_{mn,t}^0, C_{mn} p_{n,t}^0 \|_2 \le C_{mn} p_{m,t}^0 \\ p_{m,t}^0 \ge p_{n,t}^0 \end{cases} \quad \forall mn \in \Omega_{\text{NGC}} \tag{15}$$

3) Heat Network Constraints

The heat network constraints consist of the production heat of the heat source nodes and their node temperature constraint (16), the heat demand of the heat load nodes and their node temperature constraint (17), and the mixed-node hot water temperature constraint (18).

$$\begin{cases} H_{hs,t}^{\text{ss},0} = cm_{hs,t}(T_{hs,t}^{\text{ss},0} - T_{hs,t}^{\text{sr},0}) \\ T_{hs,\min}^{\text{ss}} \le T_{hs,t}^{\text{ss},0} \le T_{hs,\max}^{\text{ss}} \end{cases} \quad \forall h, hs \in \Omega_{\text{HB}} \tag{16}$$

$$\begin{cases} H_{hd,t}^{\text{hl},0} = cm_{hd,t}(T_{hd,t}^{\text{ls},0} - T_{hd,t}^{\text{lr},0}) \\ H_{hd,t}^{\text{hl},0} = H_{hd,t}^{\text{hl,p}} - \Delta H_{hd,t}^{\text{hl},0} \\ T_{hd,t}^{\text{lr},0} \le T_{hd,\max}^{\text{lr}} \end{cases} \quad \forall h, hd \in \Omega_{\text{NHB}} \tag{17}$$

$$\begin{cases} \sum_{hf\in\Omega_{\text{Se}}} T_{hf,t}^{\text{outs},0} m_{hf,t} = T_{o,t}^{\text{mixs},0} \sum_{hf\in\Omega_{\text{Se}}} m_{hf,t} \\ \sum_{hf\in\Omega_{\text{Re}}} T_{hf,t}^{\text{outr},0} m_{hf,t} = T_{o,t}^{\text{mixr},0} \sum_{hf\in\Omega_{\text{Re}}} m_{hf,t} \\ T_{hf,t}^{\text{ins},0} = T_{o,t}^{\text{mixs},0} \quad \forall hf \in \Omega_{\text{Ss}} \\ T_{hf,t}^{\text{inr},0} = T_{o,t}^{\text{mixr},0} \quad \forall hf \in \Omega_{\text{Rs}} \end{cases} \tag{18}$$

$$\begin{cases} \tau_{\text{pipe}} = \dfrac{\pi \rho_w L_{hf} d_{hf}^2}{4 m_{hf}} \\ n\Delta t \le \tau_{\text{pipe}} \le (n+1)\Delta t \end{cases} \quad \forall hf \in \Omega_{\text{R}} \bigcup \Omega_{\text{S}} \tag{19}$$

$$\begin{cases} T_{hf,t}^{\text{out},0} = K_1 T_{hf,t}^{\text{out1},0} + K_2 T_{hf,t}^{\text{out2},0} \\ K_1 + K_2 = 1 \\ \dfrac{K_1}{K_2} = \dfrac{\tau_{\text{pipe}} - n\Delta t}{(n+1)\Delta t - \tau_{\text{pipe}}} \\ T_{hf,t}^{\text{out1},0} = T_{hf,t-n\Delta t}^{\text{in},0} \\ T_{hf,t}^{\text{out2},0} = T_{hf,t-(n+1)\Delta t}^{\text{in},0} \end{cases} \quad \forall hf \in \Omega_{\text{R}} \bigcup \Omega_{\text{S}} \tag{20}$$

Equation (19) expresses τ_{pipe} in terms of unit dispatch time, placing it between $n\Delta t$ and $(n+1)\Delta t$. Equation (20) illustrates the temperature of the hot water exiting the pipeline is a linear combination of the water temperatures entering the pipeline at $n\Delta t$ and $(n+1)\Delta t$ moments in the absence of losses, where K_1 and K_2 are the respective weights. And (20) illustrates the temperature of water exiting the pipeline at time t considering the thermal inertia of heat network.

4) Equipment Constraints

The constraints on the conversion equipment and production equipment are next described. The precise expression can be found in [29].

5) Tie-line Constraints

$$\begin{cases} -P_{k,\max}^{\text{tu}} \le P_{k,t}^{\text{ut},0} \le P_{k,\max}^{\text{tu}} \\ -P_{ku,\max}^{\text{uu}} \le P_{ku,k,t}^{\text{uu},0} \le P_{ku,\max}^{\text{uu}} \end{cases} \quad \forall k, u \in \Psi^{\text{us}} \tag{21}$$

C. Intraday Adjustment Constraints

Similar to TS, intraday adjustment constraints consist of fuzzy set constraints (2)-(4) of wind power distribution and adjustment constraints. In addition to the constraints obtained after the day-ahead constraint variables are replaced with intraday scenario variables, the other related constraints are as follows. In this subsection, the definitions of the undefined variables can be found in [29].

1) Distribution Network Constraints

The electrical load limit should be less than the day-ahead load plan:

$$\Delta P_{j,t}^{\text{el},r} \le \Delta P_{j,t}^{\text{el},0} \tag{22}$$

2) Gas Network Constraints

The gas load limit must not exceed the day-ahead dispatch plan. The pressure and its rate of change at each node in the natural gas network should be maintained within controllable ranges $[-\Delta p_{m,t}^{\text{cr,max}}, \Delta p_{m,t}^{\text{cr,max}}]$ and $[-\Delta p_{m,t}^{\text{dr,max}}, \Delta p_{m,t}^{\text{dr,max}}]$, respectively, to avoid significant deviations from the day-ahead dispatch plan. In addition, the purchase volume of natural gas should vary within a specified range.

$$\Delta Q_{m,t}^{\text{gl},r} \le \Delta Q_{m,t}^{\text{gl},0} \tag{23}$$

$$\begin{cases} -\Delta p_{m,t}^{\text{cr,max}} \le p_{m,t}^r - p_{m,t-1}^r \le \Delta p_{m,t}^{\text{cr,max}} \\ -\Delta p_{m,t}^{\text{dr,max}} \le p_{m,t}^r - p_{m,t}^0 \le \Delta p_{m,t}^{\text{dr,max}} \end{cases} \tag{24}$$

$$\begin{cases} Q_{m,t}^{\text{buy},r} = Q_{m,t}^{\text{buy},0} + \Delta Q_{m,t}^{\text{buy},r+} - \Delta Q_{m,t}^{\text{buy},r-} \\ (1-\alpha_{m,t}^{\text{buy}-}) Q_{m,t}^{\text{buy},0} \le Q_{m,t}^{\text{buy},r} \le (1+\alpha_{m,t}^{\text{buy}+}) Q_{m,t}^{\text{buy},0} \end{cases} \tag{25}$$

3) Heat Network Constraints

The heat load limit should be less than that in the day-ahead dispatch plan, and the temperature fluctuation of the heat network node should be within the range of $[-\Delta T_{h,t}^{\text{sl/ch,max}}, \Delta T_{h,t}^{\text{sl/ch,max}}]$.

$$\Delta H_{h,t}^{\text{s},r} \le \Delta H_{h,t}^{\text{s},0} \tag{26}$$

$$\begin{cases} -\Delta T_{h,t}^{\text{sl,max}} \le T_{h,t}^r - T_{h,t-1}^r \le \Delta T_{h,t}^{\text{sl,max}} \\ -\Delta T_{h,t}^{\text{ch,max}} \le T_{h,t}^r - T_{h,t}^0 \le \Delta T_{h,t}^{\text{ch,max}} \end{cases} \tag{27}$$

4) Equipment Constraints

Production capacity and conversion equipment adjustments must be within a certain range.

$$\begin{cases} P_{v,t}^{\text{pro},r} = P_{v,t}^{\text{pro},0} + \Delta P_{v,t}^{\text{pro},r+} - \Delta P_{v,t}^{\text{pro},r-} \\ P_{v,t}^{\text{pro},0} - R_{v,t}^{\text{prod},0} \le P_{v,t}^{\text{pro},r} \le P_{v,t}^{\text{pro},0} + R_{v,t}^{\text{prou},0} \end{cases} \tag{28a}$$

$$\begin{cases} P_{w,t}^{\text{tra},r} = P_{w,t}^{\text{tra},0} + \Delta P_{w,t}^{\text{tra},r+} - \Delta P_{w,t}^{\text{tra},r-} \\ (1-\alpha_{w,t}^{\text{tra}}) P_{w,t}^{\text{tra},0} \le P_{w,t}^{\text{tra},r} \le (1+\alpha_{w,t}^{\text{tra}}) P_{w,t}^{\text{tra},0} \end{cases} \tag{28b}$$

V. Solution Methodology

The solution methodology for the established model primarily includes a distributed algorithm among the ESOs and a DRO within each ESO.

A. DRO of Intra-ESOs

The subproblems (SPs) of the TS and each UIES are represented as two-stage min-max-min models. We use the

C&CG algorithm to break down each ESO problem into MP and SP. The original problem can be expressed as:

$$\min_{\boldsymbol{x}^{\mathrm{ts}},\boldsymbol{x}_k^{\mathrm{us}}}\left(f^{\mathrm{ts1}}(\boldsymbol{x}^{\mathrm{ts}})+\sum_k f_k^{\mathrm{us1}}(\boldsymbol{x}_k^{\mathrm{us}})\right)+\left(\max_{\boldsymbol{p}^{\mathrm{ts}}}\min_{\boldsymbol{y}^{\mathrm{ts}}} f^{\mathrm{ts2}}(\boldsymbol{y}^{\mathrm{ts}},\boldsymbol{\mu}^{\mathrm{ts}},\boldsymbol{p}^{\mathrm{ts}})+\sum_k\max_{\boldsymbol{p}_k^{\mathrm{us}}}\min_{\boldsymbol{y}_k^{\mathrm{us}}} f_k^{\mathrm{us2}}(\boldsymbol{y}_k^{\mathrm{us}},\boldsymbol{\mu}_k^{\mathrm{us}},\boldsymbol{p}_k^{\mathrm{us}})\right) \tag{29}$$

s.t.

$$\boldsymbol{G}(\boldsymbol{x}^{\mathrm{ts}},\boldsymbol{y}^{\mathrm{ts}},\boldsymbol{\mu}^{\mathrm{ts}})\le\boldsymbol{g} \tag{30a}$$

$$\boldsymbol{H}(\boldsymbol{x}_k^{\mathrm{us}},\boldsymbol{y}_k^{\mathrm{us}},\boldsymbol{\mu}_k^{\mathrm{us}})\le\boldsymbol{h}\quad\forall k \tag{30b}$$

The problem can be divided into an MP and an SP according to the steps of C&CG algorithm [24], the expressions of which can be found in [29]. It should be noted that the probability values of the discrete scenario and intraday variables in the SP are independent of each other. We solve the inner "min" problem to obtain the optimal intraday variables for each scenario. We next address the "max" problem to derive p_i.

B. Distributed Algorithm of Inter-ESO

The conventional ADMM is limited to the convex optimization of two separable systems, and ensuring the convergence of the ADMM in multiple separable systems is challenging [31]. Thus, we employ the BADMM to address this issue. The BADMM is used to solve the MP for each ESO. The coupling constraints between the TS and UIES$_k$ as well as between UIES$_k$ and other UIESs are formulated as:

$$\boldsymbol{A}\boldsymbol{x}^{\mathrm{ts}}+\sum_{k\in\Psi^{\mathrm{us}}}\boldsymbol{B}_k\boldsymbol{x}_k^{\mathrm{us}}=\boldsymbol{0} \tag{31}$$

The BADMM requires a full-row rank matrix for the coefficient of one system variables in the coupled constraints. We introduce an extremely minimal virtual variable within the constraints among UIESs to serve as a variable for the TS, thus ensuring the applicability of the study to the BADMM. The pseudocode for the BADMM is presented in Algorithm 1.

Algorithm 1: outline of BADMM

Step 1: define the augmented Lagrange function $\boldsymbol{L}(\cdot)$. The corresponding augmented Lagrange function for MP of function (5) is given as:

$$\boldsymbol{L}(\boldsymbol{x}^{\mathrm{ts}},\boldsymbol{x}^{\mathrm{us}},\boldsymbol{\gamma})=f^{\mathrm{ts1}}+\sum_{k\in\Psi^{\mathrm{us}}}f_k^{\mathrm{us1}}+\eta^{\mathrm{ts}}+\sum_k\eta_k^{\mathrm{us}}+\boldsymbol{\gamma}^{\mathrm{T}}\left(\boldsymbol{A}\boldsymbol{x}^{\mathrm{ts}}+\sum_{k\in\Psi^{\mathrm{us}}}\boldsymbol{B}_k\boldsymbol{x}_k^{\mathrm{us}}\right)+\frac{\rho}{2}\left\|\boldsymbol{A}\boldsymbol{x}^{\mathrm{ts}}+\sum_{k\in\Psi^{\mathrm{us}}}\boldsymbol{B}_k\boldsymbol{x}_k^{\mathrm{us}}\right\|^2 \tag{32}$$

Step 2: solve the UIES$_k$ problem. Add an additional regularization term after the Lagrange function. Taking UIES$_k$ as an example, obtain the solution for the relevant variables:

$$\boldsymbol{x}_k^{\mathrm{us}(s+1)}=\arg\min_{\boldsymbol{x}_k^{\mathrm{us}}}\{\boldsymbol{L}+\Delta_\phi(\boldsymbol{x}_k^{\mathrm{us}},\boldsymbol{x}_k^{\mathrm{us}(s)})\} \tag{33}$$

Step 3: solve the TS problem. Obtain the solution for the TS variables:

$$\boldsymbol{x}^{\mathrm{ts}(s+1)}=\arg\min_{\boldsymbol{x}^{\mathrm{ts}}}\{\boldsymbol{L}+\Delta_\phi(\boldsymbol{x}^{\mathrm{ts}},\boldsymbol{x}^{\mathrm{ts}(s)})\} \tag{34}$$

Step 4: check convergence. The convergence criterion of the aforementioned problem can be expressed by the original and dual residuals via (35). If there is convergence, terminate; otherwise, go to *Step 5*.

$$\begin{cases}\varepsilon_{\mathrm{P}}^{(s+1)}=\max\left\{\left|\begin{matrix}\boldsymbol{x}^{\mathrm{ts}(s+1)}-\boldsymbol{x}_k^{\mathrm{us}(s+1)}\\ \boldsymbol{x}_k^{\mathrm{us}(s+1)}-\boldsymbol{x}_u^{\mathrm{us}(s+1)}\end{matrix}\right|_\infty\right\}\le gap_{\mathrm{P}}\\ \varepsilon_{\mathrm{D}}^{(s+1)}=\max\left\{\left|\begin{matrix}\boldsymbol{x}^{\mathrm{ts}(s+1)}-\boldsymbol{x}^{\mathrm{ts}(s)}\\ \boldsymbol{x}_k^{\mathrm{us}(s+1)}-\boldsymbol{x}_k^{\mathrm{us}(s)}\end{matrix}\right|_\infty\right\}\le gap_{\mathrm{D}}\end{cases} \tag{35}$$

Step 5: update the Lagrange multipliers. Then, return to *Step 2*. The updating rule is:

$$\boldsymbol{\gamma}^{(s+1)}=\boldsymbol{\gamma}^{(s)}+\rho\left(\boldsymbol{A}\boldsymbol{x}^{\mathrm{ts}(s+1)}+\sum_{k\in\Psi^{\mathrm{us}}}\boldsymbol{B}_k\boldsymbol{x}_k^{\mathrm{us}(s+1)}\right) \tag{36}$$

In (33), Δ_ϕ is the Bregman distance associated with the function ϕ, which can be expressed as (37). And we let $\phi(\boldsymbol{x})=\|\boldsymbol{\beta}\boldsymbol{x}\|^2$.

$$\Delta_\phi(\boldsymbol{x}_k^{\mathrm{us}},\boldsymbol{x}_k^{\mathrm{us}(s)})=\phi(\boldsymbol{x}_k^{\mathrm{us}})-\phi(\boldsymbol{x}_k^{\mathrm{us}(s)})-\left\langle\nabla\phi(\boldsymbol{x}_k^{\mathrm{us}(s)}),\boldsymbol{x}_k^{\mathrm{us}}-\boldsymbol{x}_k^{\mathrm{us}(s)}\right\rangle \tag{37}$$

C. Modified BADMM and C&CG Coordination Algorithm

In most relevant studies, an externally distributed algorithm encapsulates the internal C&CG algorithm. This methodology uses the C&CG algorithm to iteratively obtain the optimal solution of MP and SP for each ESO as well as the corresponding boundary power variables. This is followed by inter-ESO coordination using the BADMM. The distributed computation is repeated until convergence is achieved. However, convergence cannot be guaranteed. Challenges will arise, because prior to the implementation of each BADMM iteration, the probability set of worse scenarios (obtained by SP) corresponding to MP of each ESO may change after the C&CG algorithm is run. This occurs because the values of the dual and coupling variables may differ among the BADMM iterations, leading to a different objective function when C&CG algorithm is used with the iteration of each BADMM. As a result, the constraints of MP of each ESO, which are the BADMM coordinates, may continually change, making it difficult to prove the convergence of the algorithm.

1) Framework of Applied Algorithm

The pseudocode for the external C&CG algorithm with the internal BADMM is presented in Algorithm 2. The CDC manages the following measures.

Algorithm 2: external C&CG algorithm with internal BADMM

Step 1: initialize parameters. The CDC initializes parameters of the BADMM and C&CG.

Step 2: solve MP using BADMM. The CDC employs the Algorithm 1 to solve the MP of the entire system until convergence, whereas the ESO's SP is not considered. CDC obtains the lower bound LB_{sum} of the model.

$$LB_{\mathrm{sum}}^{(z)}=f^{\mathrm{ts1}(z)}+\eta^{\mathrm{ts}(z)}+\sum_{k\in\Psi^{\mathrm{us}}}(f_k^{\mathrm{us1}(z)}+\eta_k^{\mathrm{us}(z)}) \tag{38}$$

Step 3: solve SP for each ESO. The values of the MP variables obtained through *Step 2* are transmitted to each ESO.

For each ESO **do**
  Solve each ESO's SP in parallel
    If new worse wind distribution probability is obtained
    Then add probability and corresponding constraints to MP
End for
  CDC obtains the upper bound UB_{sum} of the problem:

$$UB_{\mathrm{sum}}^{(z)}=\max\left\{UB_{\mathrm{sum}}^{(z-1)},f^{\mathrm{ts1}(z)^*}+f^{\mathrm{ts2}(z)}+\sum_{k\in\Psi^{\mathrm{us}}}(f_k^{\mathrm{us1}(z)^*}+f_k^{\mathrm{us2}(z)})\right\} \tag{39}$$

Step 4: check convergence. Repeat the above steps until the convergence condition is met:

$$UB_{\mathrm{sum}}-LB_{\mathrm{sum}}\le\varepsilon_{ccg} \tag{40}$$

1) Receive tie-line power values among the ESOs, assess the BADMM convergence, and update the Lagrangian and penalty parameters.

2) Calculate the optimization results of the MP and SP of each ESO, and then determine both UB_{sum} and LB_{sum}, thereby establishing the C&CG convergence.

This paper employs the external C&CG algorithm with internal BADMM to ensure theoretical convergence.

Convergence proof: in theory, the process guarantees final convergence. As new constraints are added, the sum of MPs of all ESOs satisfies $LB_{\text{sum}}^{(z)} \geq LB_{\text{sum}}^{(z-1)}$. For the sum of SPs, it satisfies $UB_{\text{sum}}^{(z)} \leq UB_{\text{sum}}^{(z-1)}$. Thus, during the iterative process of two-stage robust problem of each ESO, the upper bound decreases, the lower bound increases, and both the upper and lower bounds converge, thus ensuring that the optimization problem for the entire system converges. When the BADMM has high convergence precision, its solution error has a negligible influence on the adverse wind power probability distribution generated by the SP. Consequently, using the BADMM does not significantly affect C&CG convergence.

2) Acceleration Strategy

The BADMM has a clear structure that facilitates the design of acceleration strategies. To expedite the BADMM convergence, we propose the following strategies.

1) Note that the initial values of the coupling and dual variables significantly affect BADMM convergence, we use those from the previous C&CG iteration as the initial conditions for the subsequent C&CG iteration.

2) We apply a dynamic update method for parameters β and ρ. Adjusting ρ based on the original residual behavior improves convergence, whereas β is adjusted based on the iteration of the dual residual. The optimal values for both parameters are determined accordingly. Simultaneously, the residual value of the current round is compared with that prior to the S^{th} iteration. Herein, $\lambda_1 > 1$, $\lambda_2 < 1$, and $\lambda_3 > 1$ are the parameter variation factors, and $\tau_1 > 1$, $\tau_2 > 1$, $\tau_3 < 1$, and $\tau_4 > 1$ are the comparison parameters.

$$\begin{cases} \rho^{(s+1)} = \lambda_1 \rho^{(s)} & \varepsilon_{\text{P}}^{(s+1)} \geq \tau_1 \varepsilon_{\text{P}}^{(s-S)},\ \varepsilon_{\text{P}}^{(s+1)} \geq \tau_2 \varepsilon_{\text{D}}^{(s)} \\ \rho^{(s+1)} = \lambda_2 \rho^{(s)} & \varepsilon_{\text{P}}^{(s+1)} \leq \tau_3 \varepsilon_{\text{D}}^{(s)} \\ \rho^{(s+1)} = \rho^{(s)} & \text{otherwise} \end{cases} \tag{41}$$

$$\begin{cases} \beta^{(s+1)} = \lambda_3 \beta^{(s)} & \varepsilon_{\text{D}}^{(s+1)} \geq \tau_4 \varepsilon_{\text{D}}^{(s-S)} \\ \beta^{(s+1)} = \beta^{(s)} & \text{otherwise} \end{cases} \tag{42}$$

VI. Case Studies

In this paper, cases are solved using the Gurobi 9.5 solver in a Python 3.8 environment and executed on a computer with an Intel i7-12700 CPU and 16 GB RAM.

A. Tests on an IEEE 6-bus TS and Two UIESs

The test system is shown in Fig. 2. We construct the system using an IEEE 6-bus TS and two UIESs, where the urban energy systems consist of a heat network with 6 nodes, a gas network with 7 nodes, and a distribution network with 7 nodes. For each energy system, we select 5 intraday wind scenarios for optimization. The parameters of the TS, distribution network, heat network, natural gas network, equipment, wind forecast, and intraday scenarios of each ESO are presented in [29]. The gap_{D} and gap_{P} of the BADMM are both set to be 0.02 MW, and the convergence accuracy ε_{ccg} of C&CG is 0.2 MW.

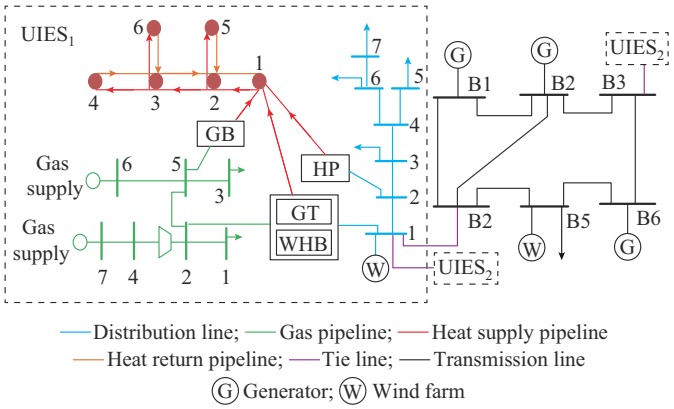

Fig. 2. Test system.

1) Comparison of Different Coordinating Models

To illustrate the advantages of coordination across energy systems and the tight integration of diverse energy sources, the following comparison models are constructed. ① Model 1: each system is independently optimized. ② Model 2: electrical-heat coupling is ignored. ③ Model 3: interconnection model proposed in this paper.

1) Comparison of Models 1-3

A comparison of Models 1-3 highlights the advantages of the interconnection between ESOs. Table II lists the operating costs of different models in the day-ahead and intraday stages.

TABLE II
Comparisons of Model Optimization Results

Model	TS cost ($)		$UIES_1$ cost ($)		$UIES_2$ cost ($)		Total cost ($)	Gas purchase (m^3)	Wind curtailment (MWh)	Power generation of generator (MWh)
	Day-ahead	Intraday	Day-ahead	Intraday	Day-ahead	Intraday				
Model 1	18612.9	107.5	23534.6	6302.2	31617.9	12025.1	121136.9	181030.6	133.7	3188.6
Model 2	24351.4	1316.5	20565.0	4084.0	23345.9	3937.1	82592.4	184995.0	25.0	3983.2
Model 3	27387.7	1375.6	19018.6	3363.5	21577.4	3728.3	79389.8	170723.2	0	4478.5

Overall, the total dispatch cost follows the order Model 3 < Model 2 < Model 1. Figure 3 and Table II show that Model 1 has significant wind curtailment in intraday scenarios, indicating that Model 3 not only outperforms Model 1 in terms of cost control but also promotes wind consumption in different intraday scenarios. Note that "1-5" in Fig. 3 represent the five intraday scenarios. The benefits of interconnected dispatch are further illustrated when combined with day-ahead dispatch results, as shown in Fig. 4. As Fig. 4(b) and (c) shows, the TS typically represents the net power output side in Models 2 and 3 due to surplus power. By contrast, Model 1, with isolated ESO dispatch, reduces the power out-

put of generators in the TS and leads to wind curtailment.

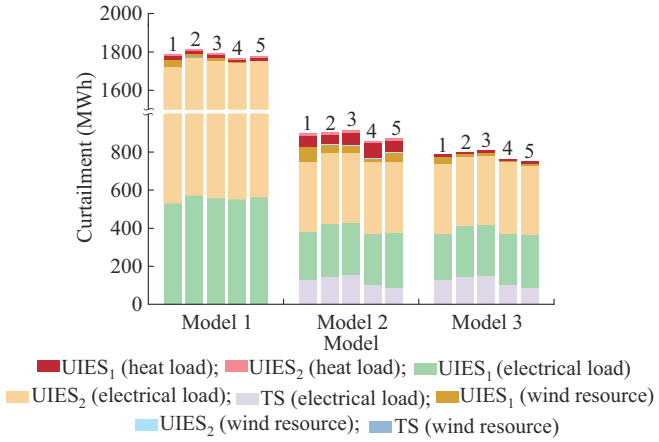

Fig. 3. Intraday wind and load curtailments in Models 1-3.

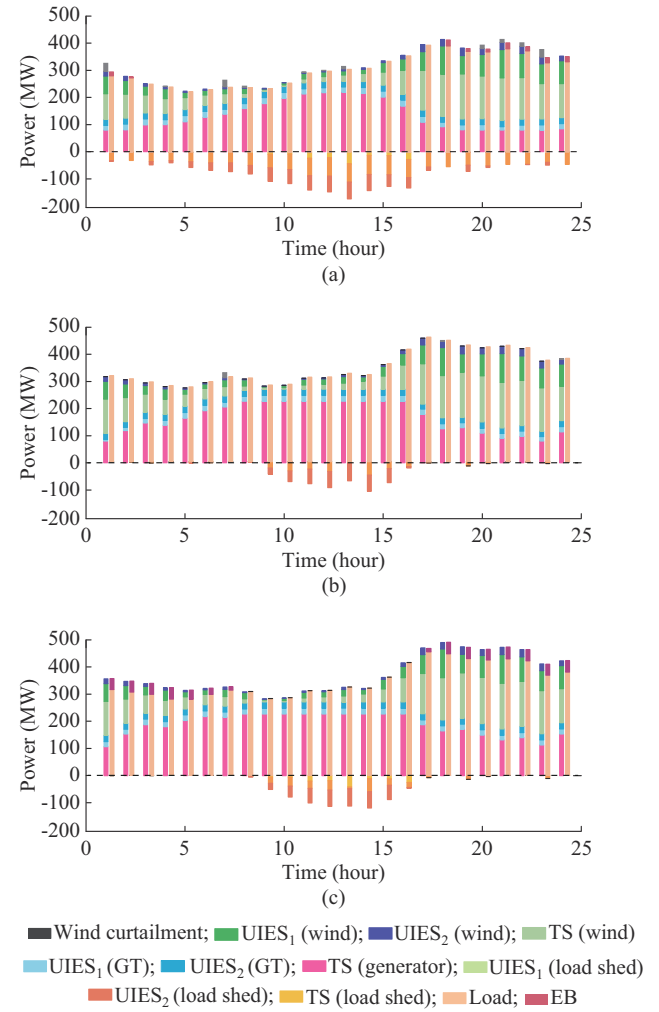

Fig. 4. Power and load optimization results of Models 1-3. (a) Model 1. (b) Model 2. (c) Model 3.

In terms of energy consumption, $UIES_1$ and $UIES_2$ exhibit more severe load limitations due to the lack of TS support, as shown in Figs. 3 and 4. The full interconnection strategy can achieve day-ahead planned power allocation and account for unfavorable scenarios within the day.

In terms of privacy protection, the interconnection method of Model 3 enables direct transactions between UIESs without TS involvement, which is favorable for privacy protection.

In Models 1-3, significant load limits occur during periods 9-16 in Fig. 4. Because of the reduced wind power, generator units operate close to full power but still cannot meet the load demand. In future systems with a high proportion of renewable energy, orderly power consumption will become necessary during periods of wind power shortage.

2) Comparison of Models 2 and 3

A comparison of Models 2 and 3 emphasizes the effects of energy coupling on wind power consumption. In Model 2, electricity and heat are not connected. Therefore, the heat load can only be provided by WHBs and GBs, and low-cost wind and thermal power conversion to heat cannot be utilized. Table II demonstrates that in Model 2, power generation of the generators decreases and purchased natural gas increases, resulting in higher energy costs. In addition, Fig. 3 reveals that due to the decoupling of electricity and heat, the system faces a heat load deficiency in each wind scenario within the day, and UIES experiences higher amount of wind curtailment. Thus, deep coupling between different energy forms can enhance the conversion and improve overall energy utilization.

2) Decentralization Convergence Analysis

Three comparative models are established to verify the effectiveness of Algorithm 2. ① Model 4: BADMM without acceleration strategy. ② Model 5: external BADMM with internal C&CG. ③ Model 6: centralized method.

In this paper, the C&CG serves as the external framework, whereas the BADMM constitutes the internal implementation mechanism.

1) Comparison of Models 3 and 4

The evolutions of UB_{sum} and LB_{sum} in C&CG of Models 3 and 4 are illustrated in Figs. 5 and 6, respectively. After two C&CG iterations, both the models converge.

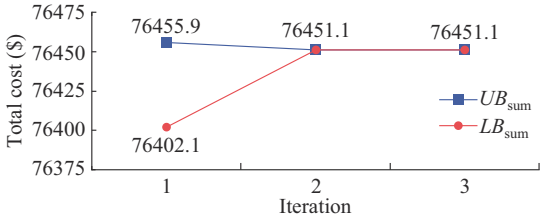

Fig. 5. Evolution of UB_{sum} and LB_{sum} in C&CG of Model 3.

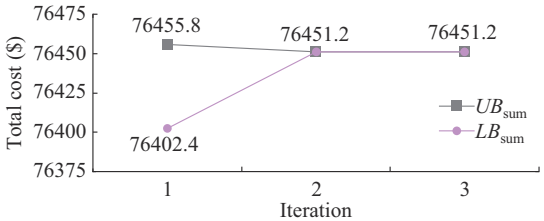

Fig. 6. Evolution of UB_{sum} and LB_{sum} in C&CG of Model 4.

Figure 7 displays the maximum residual evolution in BADMM of MP of Models 3 and 4. In the first C&CG itera-

tion, Model 3 under variable parameters shows a fluctuating maximum residual as compared with the non-accelerating strategy in Model 4. However, the overall trend converges with fewer iterations. The method in Model 3 avoids a slow decrease in the maximum residual and helps determine ρ and β for subsequent iterations.

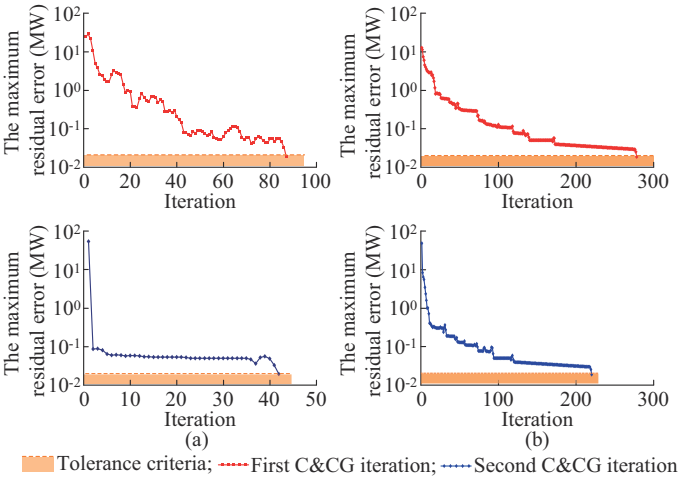

Fig. 7. The maximum residual error in BADMM of MP of Models 3 and 4. (a) Model 3. (b) Model 4.

In each C&CG iteration of Model 4, the initial parameter values of the BADMM remain the same. In the first two C&CG iterations of Model 4, the BADMM converges after 278 and 220 iterations, respectively. Although more iterations are required, a higher accuracy is achieved. Notably, the solution time is not directly proportional to the total number of C&CG iterations. As constraints and scenario probability variables are added to the MP, the solution time for the next iteration of C&CG increases. The first C&CG iteration of Model 3 requires more time to obtain the optimization results and variables. By using the coupling variables, Lagrange multipliers, the penalty parameters from the first C&CG iteration as the initial conditions for the subsequent iteration, and the BADMM convergence iterations for the MP are significantly reduced. In the first two C&CG iterations of Model 3, the BADMM converges after only 87 and 42 iterations, respectively.

Table III shows that the final convergence accuracy of the distributed algorithm is reliable. The solution result for Model 6 is \$76440.8 compared with that of the centralized optimization, and the errors for the optimization results of Models 3 and 4 are minimal. Although Model 3 requires more computational time than Model 6, the significance of the distributed optimization method utilized in this paper is maintained because of its advantages of decentralization, data privacy, security, and scalability.

2) Comparison of Models 3 and 5

As Fig. 8 and Table III show, Model 5 achieves a convergence precision of 0.1 MW after 83 iterations but still has a longer solution time as compared with that of Model 3. This is because the MP of each ESO is determined using the iterative C&CG algorithm, which implies that the solution time for each BADMM iteration is longer. Furthermore, during the BADMM coordination for solving each MP for ESO, the adverse probability sets of wind scenarios in different BADMM iterations might vary. Consequently, the constraints of each MP may undergo continuous adjustments, making it challenging to prove the convergence of Model 5.

TABLE III
COMPARISONS OF MODELS 3-5

Model	Time (s)	The maximum residual (MW)	Total cost (\$)
Model 3	174.9	0.02	76451.1
Model 4	752.2	0.02	76451.2
Model 5	467.4	0.10	76458.9

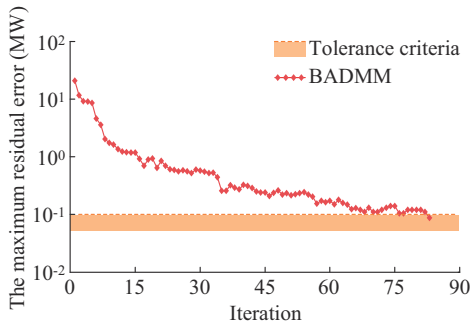

Fig. 8. Evolution of the maximum residual error in BADMM of MP of Model 5.

3) Comparison of Uncertainty Models

The following models are established for comparison to illustrate the efficacy of the DRO method. Model 7 represents stochastic optimization (SO) algorithm and Model 8 represents RO algorithm. SO adopts the same intraday scenarios as DRO with a fixed probability of 0.2 for each scenario possibility. RO employs the method described in [32], and the wind power boundary is consistent with the aforementioned conditions.

Reference [29] shows that the primary difference in dispatch costs lies in intraday adjustments, with the DRO costs falling between those of SO and conventional RO. DRO maintains a degree of conservatism, balancing economy and conservatism based on the wind power probability distribution.

Figure 9 displays the relationship between total cost and parameters θ_1 and θ_∞. Under a fixed θ_∞, the system dispatch cost increases as θ_1 rises because the allowed probability deviation range for intraday scenarios expands, generating worse intraday wind scenario probability distributions and rising costs. With a fixed θ_1, the cost first exhibits a rising and then a flat pattern. This occurs because when $\theta_1 \geq \theta_\infty$, increasing θ_∞ produces a worse probability distribution; whereas when $\theta_1 < \theta_\infty$, the cost remains unchanged (as θ_∞ cannot exceed θ_1) with the maximum cost at $\theta_1 = \theta_\infty$. The cost results obtained from DRO are lower than those obtained from RO, further confirming that DRO is less conservative than RO.

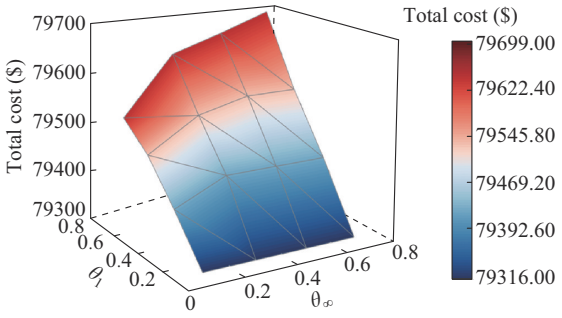

Fig. 9. Relationship between total cost and parameters θ_1 and θ_∞.

B. Scalability Test

To further demonstrate the effectiveness of Algorithm 2 in practical cases, a large-scale test is conducted using the 10 UIESs, which are identical in configuration and are connected to the IEEE 118-bus transmission network. The boundary buses are 18, 32, 34, 40, 55, 70, 74, 77, 92, and 112 of the TS, with each adjacent serial number of the UIESs interconnected. For the larger model, a relatively high convergence accuracy is set to balance the solution efficiency. The convergence residual in the BADMM is 0.05 MW and that of the C&CG algorithm is 0.2 MW. Figure 10 shows the evolution of UB_{sum} and LB_{sum} in C&CG, and Fig. 11 presents the evolution of total cost of BADMM in the first and second C&CG iterations.

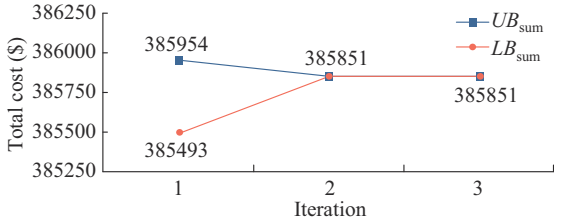

Fig. 10. Evolution of UB_{sum} and LB_{sum} in C&CG.

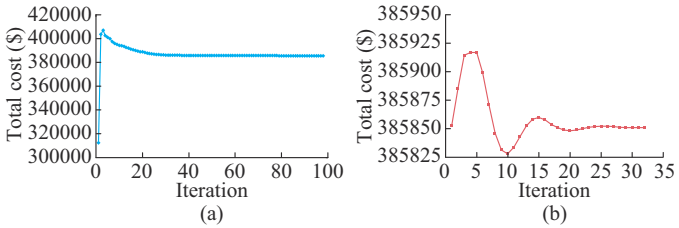

Fig. 11. Evolution of total cost of BADMM in first and second C&CG iterations. (a) First iteration. (b) Second iteration.

The optimization results show that the problem converges after two C&CG iterations.

The BADMM of the MP converges after 98 and 32 iterations. Because of the lower convergence precision of the BADMM, the number of final convergence iterations is relatively low, and the final solution time is 943.2 s. As the model scale expands, each iteration in the BADMM takes longer time. However, the solution time for day-ahead large-scale interconnected dispatch is acceptable. In this paper, each ESO's interior is represented by a convex model, leading to a rapid solution speed when solving each ESO model. Most of the solution time is spent on the convergence of the distributed algorithm. Therefore, the convergence accuracy of the BADMM should be set appropriately based on actual circumstances, allowing for some compromise in the convergence accuracy for large-scale systems.

VII. Conclusion

This paper presents a day-ahead coordinated optimization model based on DRO for a fully interconnected TS and UIESs. First, the traditional power transmission and distribution interconnection is expanded to encompass the TS and UIESs using the BADMM (suitable for multi-block problems), thereby ensuring the privacy of each ESO. Second, due to the increased uncertainty of wind power, deterministic dispatch strategies have proven unsatisfactory. Accordingly, the developed DRO balances economy and conservativeness. Finally, an accelerated external C&CG with internal BADMM is designed, offering theoretical convergence guarantees and improved solution rates compared with existing distributed robust methods. Small-scale cases demonstrate the advantages of various energy coupling and interconnected models for enhancing wind energy consumption and addressing uncertainty. Large-scale cases reveal the applicability of the model to engineering applications. This paper focuses on cost optimization across all ESOs and does not consider individual ESO benefit improvements from interconnections. Future research could include cooperative game-based benefit improvements for each ESO in decision-making.

References

[1] P. Li, Q. Wu, M. Yang *et al.*, "Distributed distributionally robust dispatch for integrated transmission-distribution systems," *IEEE Transactions on Power Systems*, vol. 36, no. 2, pp. 1193-1205, Mar. 2021.

[2] Y. Ji, Q. Xu, and Y. Xia, "Distributed robust energy and reserve dispatch for coordinated transmission and active distribution systems," *Journal of Modern Power Systems and Clean Energy*, vol. 11, no. 5, pp. 1494-1506, Sept. 2023.

[3] Z. Chen, Z. Li, C. Guo *et al.*, "Fully distributed robust reserve scheduling for coupled transmission and distribution systems," *IEEE Transactions on Power Systems*, vol. 36, no. 1, pp. 169-182, Jan. 2021.

[4] H. Gao, S. Xu, Y. Liu *et al.*, "Decentralized optimal operation model for cooperative microgrids considering renewable energy uncertainties," *Applied Energy*, vol. 262, p. 114579, Mar. 2020.

[5] H. Gao, J. Liu, L. Wang *et al.*, "Decentralized energy management for networked microgrids in future distribution systems," *IEEE Transactions on Power Systems*, vol. 33, no. 4, pp. 3599-3610, Jul. 2018.

[6] W. Gan, M. Yan, W. Yao *et al.*, "Decentralized computation method for robust operation of multi-area joint regional-district integrated energy systems with uncertain wind power," *Applied Energy*, vol. 298, p. 117280, Sept. 2021.

[7] F. Chen, H. Deng, Y. Chen *et al.*, "Distributed robust cooperative scheduling of multi-region integrated energy system considering dynamic characteristics of networks," *International Journal of Electrical Power & Energy Systems*, vol. 145, p. 108605, Feb. 2023.

[8] G. Pan, W. Gu, S. Zhou *et al.*, "Synchronously decentralized adaptive robust planning method for multi-stakeholder integrated energy systems," *IEEE Transactions on Sustainable Energy*, vol. 11, no. 3, pp. 1128-1139, Jul. 2020.

[9] H. Qiu, W. Gu, Y. Xu *et al.*, "Robustly multi-microgrid scheduling: stakeholder-parallelizing distributed optimization," *IEEE Transactions on Sustainable Energy*, vol. 11, no. 2, pp. 988-1001, Jul. 2020.

[10] C. Lv, R. Liang, and Y. Chai, "Decentralized bilateral risk-based self-healing strategy for power distribution network with potentials from central energy stations," *Journal of Modern Power Systems and Clean Energy*, vol. 11, no. 1, pp. 179-190, Jan. 2023.

[11] J. Zhai, Y. Jiang, J. Li *et al.*, "Distributed adjustable robust optimal

power-gas flow considering wind power uncertainty," *International Journal of Electrical Power & Energy Systems*, vol. 139, p. 107963, Jul. 2022.
[12] T. Jiang, C. Wu, R. Zhang *et al*., "Risk-averse TSO-DSOs coordinated distributed dispatching considering renewable energy and demand response uncertainties," *Applied Energy*, vol. 327, p. 120024, Dec. 2022.
[13] C. Chen, B. He, Y. Ye *et al*., "The direct extension of ADMM for multi-block convex minimization problems is not necessarily convergent," *Mathematical Programming*, vol. 155, pp. 57-79, Jan. 2016.
[14] B. He, M. Tao, and X. Yuan, "A splitting method for separable convex programming," *IMA Journal of Numerical Analysis*, vol. 35, no. 1, pp. 394-426, Jan. 2015.
[15] J. Zhong, Y. Cao, Y. Li *et al*., "Distributed modeling considering uncertainties for robust operation of integrated energy system," *Energy*, vol. 224, p. 120179, Jun. 2021.
[16] M. H. Ullah and J.-D. Park, "Transactive energy market operation through coordinated TSO-DSOs-DERs interactions," *IEEE Transactions on Power Systems*, vol. 38, no. 2, pp. 1978-1990, Mar. 2023.
[17] B. Wang, C. Zhang, C. Li *et al*., "Transactive energy sharing in a microgrid via an enhanced distributed adaptive robust optimization approach," *IEEE Transactions on Smart Grid*, vol. 13, no. 3, pp. 2279-2293, May 2022.
[18] Y. Zhang, J. Le, F. Zheng *et al*., "Two-stage distributionally robust coordinated scheduling for gas-electricity integrated energy system considering wind power uncertainty and reserve capacity configuration," *Renewable Energy*, vol. 135, pp. 122-135, May 2019.
[19] C. Chen, X. Wu, Y. Li *et al*., "Distributionally robust day-ahead scheduling of park-level integrated energy system considering generalized energy storages," *Applied Energy*, vol. 302, p. 117493, Nov. 2021.
[20] J. Liu, Y. Chen, C. Duan *et al*., "Distributionally robust optimal reactive power dispatch with Wasserstein distance in active distribution network," *Journal of Modern Power Systems and Clean Energy*, vol. 8, no. 3, pp. 426-436, May 2020.
[21] T. Ding, Q. Yang, Y. Yang *et al*., "A data-driven stochastic reactive power optimization considering uncertainties in active distribution networks and decomposition method," *IEEE Transactions on Smart Grid*, vol. 9, no. 5, pp. 4994-5004, Sept. 2018.
[22] C. Wang, S. Wang, F. Liu *et al*., "Risk-loss coordinated admissibility assessment of wind generation for integrated electric-gas systems," *IEEE Transactions on Smart Grid*, vol. 11, no. 5, pp. 4454-4465, Sept. 2020.
[23] M. Yan, N. Zhang, X. Ai *et al*., "Robust two-stage regional-district scheduling of multi-carrier energy systems with a large penetration of wind power," *IEEE Transactions on Sustainable Energy*, vol. 10, no. 3, pp. 1227-1239, Jul. 2019.
[24] B. Zeng and L. Zhao, "Solving two-stage robust optimization problems using a column-and-constraint generation method," *Operations Research Letters*, vol. 41, no. 5, pp. 457-461, Sept. 2013.
[25] J. Zhai, M. Zhou, J. Li *et al*., "Hierarchical and robust scheduling approach for VSC-MTDC meshed AC/DC grid with high share of wind power," *IEEE Transactions on Power Systems*, vol. 36, no. 1, pp. 793-805, Jan. 2021.
[26] S. Sharma, A. Verma, and B. K. Panigrahi, "Robustly coordinated distributed voltage control through residential demand response under multiple uncertainties," *IEEE Transactions on Industry Applications*, vol. 57, no. 4, pp. 4042-4058, Aug. 2021.
[27] K. Zhou, Z. Fei, and R. Hu, "Hybrid robust decentralized optimization of emission-aware multi-energy microgrids considering multiple uncertainties," *Energy*, vol. 265, p. 126405, Feb. 2023.
[28] C. He, L. Wu, T. Liu *et al*., "Robust co-optimization scheduling of electricity and natural gas systems via ADMM," *IEEE Transactions on Sustainable Energy*, vol. 8, no. 2, pp. 658-670, Apr. 2017.
[29] W. Xu. (2024, Apr.). Test data for cases. [Online]. Available: https://github.com/neverba/Data.
[30] Y. He, M. Shahidehpour, Z. Li *et al*., "Robust constrained operation of integrated electricity-natural gas system considering distributed natural gas storage," *IEEE Transactions on Sustainable Energy*, vol. 9, no. 3, pp. 1061-1071, Jul. 2018.
[31] F. Wang, W. Cao, and Z. Xu, "Convergence of multi-block Bregman ADMM for nonconvex composite problems," *Science China Information Sciences*, vol. 61, pp. 1-12, Jun. 2018.
[32] Y. Ji, Q. Xu, and L. Sun, "Distributed robust dispatch for the coordination of transmission and distribution systems considering air conditioning loads," *International Journal of Electrical Power & Energy Systems*, vol. 148, p. 108932, Jun. 2023.

Wei Xu received the B.S. degree in electrical engineering from Shandong University, Jinan, China, in 2020, and the M.S. degree in electrical engineering from Harbin Institute of Technology (HIT), Harbin, China, in 2022. He is currently pursuing the Ph.D. degree at HIT. His research interests include coordinated optimization of energy systems.

Yufeng Guo received the B.S., M.S., and Ph.D. degrees in power machinery and engineering from the School of Energy Science and Engineering, Harbin Institute of Technology (HIT), Harbin, China, in 1999, 2001, and 2005, respectively. She currently serves as a Professor and the Deputy Director of the Power Systems Research Institute at School of Electrical Engineering, HIT. Her research interests include power system stability and power system modeling and simulation.

Tianhui Meng received the B.S. and M.S. degrees in electrical engineering from Harbin Institute of Technology (HIT), Harbin, China, in 2016 and 2019, respectively. She is currently pursuing the Ph.D. degree at HIT. Her research interests include microgrid control and optimization.

Yingwei Wang received the M.S. degree in electrical engineering from Shenyang University of Technology, Shenyang, China, in 2020. He is currently pursuing the Ph.D. degree at Harbin Institute of Technology, Harbin, China. His research interests include wind power optimization and fatigue load control of wind turbines.

Jilai Yu received the B.S. and M.S. degrees from Harbin Institute of Technology (HIT), Harbin, China, in 1988 and 1990, respectively, and the Ph.D. degree from North China Institute of Electric Power, Beijing, China, in 1992. He has been a Professor in the Department of Electrical Engineering at HIT since 1998. His current research interests include power system analysis and control as well as optimal dispatch of power systems.